

Automation of the leading order calculations for $e^+e^- \rightarrow$ hadrons

Karol Kołodziej

Institute of Physics
University of Silesia
Katowice

Radio Monte Carlo Working Group meeting

Frascati, 18 – 19 November, 2014

Motivation

The knowledge of $\sigma_{e^+e^- \rightarrow \text{hadrons}}(s)$ allows, through dispersion relations, for determination of **hadronic contributions to the vacuum polarization**.

⇒ Better precision of theoretical predictions for the **muon anomalous magnetic moment** and **evolution of the fine structure constant** from the Thomson limit to high energy scales.

Motivation

The knowledge of $\sigma_{e^+e^- \rightarrow \text{hadrons}}(s)$ allows, through dispersion relations, for determination of **hadronic contributions to the vacuum polarization**.

⇒ Better precision of theoretical predictions for the **muon anomalous magnetic moment** and **evolution of the fine structure constant** from the Thomson limit to high energy scales.

Below the J/ψ threshold, $\sigma_{e^+e^- \rightarrow \text{hadrons}}(s)$ must be measured, either by the **initial beam energy scan** or with the use of a **radiative return method**, and compared with predictions of a Monte Carlo program, as e.g. PHOKARA.

Motivation

The knowledge of $\sigma_{e^+e^- \rightarrow \text{hadrons}}(s)$ allows, through dispersion relations, for determination of **hadronic contributions to the vacuum polarization**.

⇒ Better precision of theoretical predictions for the **muon anomalous magnetic moment** and **evolution of the fine structure constant** from the Thomson limit to high energy scales.

Below the J/ψ threshold, $\sigma_{e^+e^- \rightarrow \text{hadrons}}(s)$ must be measured, either by the **initial beam energy scan** or with the use of a **radiative return method**, and compared with predictions of a Monte Carlo program, as e.g. PHOKARA.

To reach the desired precision level, **radiative corrections must be included in the predictions**.

Motivation

The knowledge of $\sigma_{e^+e^- \rightarrow \text{hadrons}}(s)$ allows, through dispersion relations, for determination of **hadronic contributions to the vacuum polarization**.

⇒ Better precision of theoretical predictions for the **muon anomalous magnetic moment** and **evolution of the fine structure constant** from the Thomson limit to high energy scales.

Below the J/ψ threshold, $\sigma_{e^+e^- \rightarrow \text{hadrons}}(s)$ must be measured, either by the **initial beam energy scan** or with the use of a **radiative return method**, and compared with predictions of a Monte Carlo program, as e.g. PHOKARA.

To reach the desired precision level, radiative corrections must be included in the predictions.

However, if the number of particles in the final state is big

⇒ **the number of Feynman diagrams becomes large**, but the cross section is small,

Motivation

The knowledge of $\sigma_{e^+e^- \rightarrow \text{hadrons}}(s)$ allows, through dispersion relations, for determination of **hadronic contributions to the vacuum polarization**.

⇒ Better precision of theoretical predictions for the **muon anomalous magnetic moment** and **evolution of the fine structure constant** from the Thomson limit to high energy scales.

Below the J/ψ threshold, $\sigma_{e^+e^- \rightarrow \text{hadrons}}(s)$ must be measured, either by the **initial beam energy scan** or with the use of a **radiative return method**, and compared with predictions of a Monte Carlo program, as e.g. PHOKARA.

To reach the desired precision level, radiative corrections must be included in the predictions.

However, if the number of particles in the final state is big

⇒ **the number of Feynman diagrams becomes large**, but the cross section is small,

⇒ **it can be useful to have at least the leading order (LO) predictions** for the reactions of interest.

Motivation

The knowledge of $\sigma_{e^+e^- \rightarrow \text{hadrons}}(s)$ allows, through dispersion relations, for determination of **hadronic contributions to the vacuum polarization**.

⇒ Better precision of theoretical predictions for the **muon anomalous magnetic moment** and **evolution of the fine structure constant** from the Thomson limit to high energy scales.

Below the J/ψ threshold, $\sigma_{e^+e^- \rightarrow \text{hadrons}}(s)$ must be measured, either by the **initial beam energy scan** or with the use of a **radiative return method**, and compared with predictions of a Monte Carlo program, as e.g. PHOKARA.

To reach the desired precision level, radiative corrections must be included in the predictions.

However, if the number of particles in the final state is big

⇒ **the number of Feynman diagrams becomes large**, but the cross section is small,

⇒ **it can be useful to have at least the leading order (LO) predictions** for the reactions of interest.

At low energies, the hadronic final states consist mostly of pions or kaons, accompanied by one or more photons.

Light fermion pairs, as e^+e^- , $\mu^+\mu^-$ or $\bar{N}N$, can also be present.

At low energies, the hadronic final states consist mostly of pions or kaons, accompanied by one or more photons.

Light fermion pairs, as e^+e^- , $\mu^+\mu^-$ or $\bar{N}N$, can also be present.

Because of that diversity of particles and large number of the diagrams, it is desirable to employ automatic, general purpose Monte Carlo tools.

At low energies, the hadronic final states consist mostly of pions or kaons, accompanied by one or more photons.

Light fermion pairs, as e^+e^- , $\mu^+\mu^-$ or $\bar{N}N$, can also be present.

Because of that diversity of particles and large number of the diagrams, it is desirable to employ automatic, general purpose Monte Carlo tools.

carlomat is a program for automatic computation of the lowest order cross sections of multiparticle reactions,

At low energies, the hadronic final states consist mostly of pions or kaons, accompanied by one or more photons.

Light fermion pairs, as e^+e^- , $\mu^+\mu^-$ or $\bar{N}N$, can also be present.

Because of that diversity of particles and large number of the diagrams, it is desirable to employ automatic, general purpose Monte Carlo tools.

carlomat is a program for automatic computation of the lowest order cross sections of multiparticle reactions, which originally was dedicated mainly to description of the processes of production and decay of heavy particles such as, e.g., top quarks, Higgs boson, or electroweak gauge bosons.

At low energies, the hadronic final states consist mostly of pions or kaons, accompanied by one or more photons.

Light fermion pairs, as e^+e^- , $\mu^+\mu^-$ or $\bar{N}N$, can also be present.

Because of that diversity of particles and large number of the diagrams, it is desirable to employ automatic, general purpose Monte Carlo tools.

carlomat is a program for automatic computation of the lowest order cross sections of multiparticle reactions, which originally was dedicated mainly to description of the processes of production and decay of heavy particles such as, e.g., top quarks, Higgs boson, or electroweak gauge bosons.

Version 2 of carlomat was released in summer 2013 and the paper: KK, *Comput. Phys. Commun.* **185** (2014) 323, [arXiv:1305.5096], was published in the beginning of 2014.

Substantial modifications with respect to version 1 of the program include:

Version 2 of carlomat was released in summer 2013 and the paper: KK, *Comput. Phys. Commun.* **185** (2014) 323, [arXiv:1305.5096],

was published in the beginning of 2014.

Substantial modifications with respect to version 1 of the program include:

- generation of a single phase space parameterization for the Feynman diagrams of the same topology,

Version 2 of carlomat was released in summer 2013 and the paper: KK, *Comput. Phys. Commun.* **185** (2014) 323, [arXiv:1305.5096],

was published in the beginning of 2014.

Substantial modifications with respect to version 1 of the program include:

- generation of a single phase space parameterization for the Feynman diagrams of the same topology,
- an interface to parton density functions,

Version 2 of carlomat was released in summer 2013 and the paper: [KK, Comput. Phys. Commun. **185** \(2014\) 323, \[arXiv:1305.5096\]](#),

was published in the beginning of 2014.

Substantial modifications with respect to version 1 of the program include:

- generation of a single phase space parameterization for the Feynman diagrams of the same topology,
- an interface to parton density functions,
- improvement of the color matrix computation,
- the Cabibbo-Kobayashi-Maskawa mixing in the quark sector,

Version 2 of carlomat was released in summer 2013 and the paper: [KK, Comput. Phys. Commun. **185** \(2014\) 323, \[arXiv:1305.5096\]](#),

was published in the beginning of 2014.

Substantial modifications with respect to version 1 of the program include:

- generation of a single phase space parameterization for the Feynman diagrams of the same topology,
- an interface to parton density functions,
- improvement of the color matrix computation,
- the Cabibbo-Kobayashi-Maskawa mixing in the quark sector,
- effective models, including scalar electrodynamics, the Wtb interaction with operators of dimension up to 5 and a general top-Higgs coupling.

Version 2 of carlomat was released in summer 2013 and the paper: [KK, Comput. Phys. Commun. 185 \(2014\) 323, \[arXiv:1305.5096\]](#),

was published in the beginning of 2014.

Substantial modifications with respect to version 1 of the program include:

- generation of a single phase space parameterization for the Feynman diagrams of the same topology,
- an interface to parton density functions,
- improvement of the color matrix computation,
- the Cabibbo-Kobayashi-Maskawa mixing in the quark sector,
- effective models, including scalar electrodynamics, the Wtb interaction with operators of dimension up to 5 and a general top-Higgs coupling.

Article Usage Dashboard



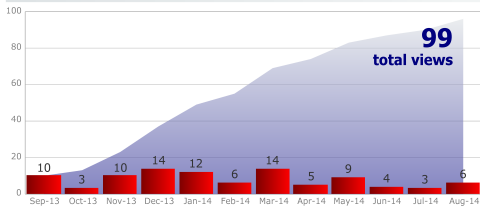
carlomat, version 2 of the program for automatic computation of lowest order cross sections

Kolodziej, K.

Computer Physics Communications, Volume(s) 185, 04-Sep-2013, Pages 323-329

[View Article](#)

Trend and cumulative views



Copyright © 2013 Elsevier B.V. All rights reserved.

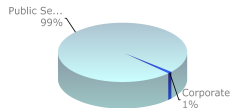
[Terms and conditions](#)

[Support](#)

Views by geography

Top countries	Rank	Views	Pct
United States	1	26	26%
China	2	24	24%
Poland	3	11	11%
India	4	6	6%
Germany	5	4	4%

Corporate versus Public Sector



Anomalous Wtb coupling

The effective Lagrangian of the Wtb interaction containing operators of dimension four and five has the following form:

$$L_{Wtb} = \frac{g}{\sqrt{2}} V_{tb} \left[W_{\mu}^{-} \bar{b} \gamma^{\mu} \left(f_1^L P_L + f_1^R P_R \right) t - \frac{1}{m_W} \partial_{\nu} W_{\mu}^{-} \bar{b} \sigma^{\mu\nu} \left(f_2^L P_L + f_2^R P_R \right) t \right] + \text{h.c.}$$

Couplings $f_i^L, f_i^R, i = 1, 2$, can be complex in general. In the SM, $f_1^L = 1$ and other couplings are 0.

Anomalous Wtb coupling

The effective Lagrangian of the Wtb interaction containing operators of dimension four and five has the following form:

$$L_{Wtb} = \frac{g}{\sqrt{2}} V_{tb} \left[W_{\mu}^{-} \bar{b} \gamma^{\mu} \left(f_1^L P_L + f_1^R P_R \right) t \right. \\ \left. - \frac{1}{m_W} \partial_{\nu} W_{\mu}^{-} \bar{b} \sigma^{\mu\nu} \left(f_2^L P_L + f_2^R P_R \right) t \right] + \text{h.c.}$$

Couplings $f_i^L, f_i^R, i = 1, 2$, can be complex in general. In the SM, $f_1^L = 1$ and other couplings are 0.

The EM interaction of spin 1/2 nucleons has a similar form:

$$L_{\gamma NN} = e A_{\mu} \bar{N}(p') \left[\gamma^{\mu} F_1(Q^2) + \frac{i}{2m_N} \sigma^{\mu\nu} q_{\nu} F_2(Q^2) \right] N(p).$$

Anomalous Wtb coupling

The effective Lagrangian of the Wtb interaction containing operators of dimension four and five has the following form:

$$L_{Wtb} = \frac{g}{\sqrt{2}} V_{tb} \left[W_{\mu}^{-} \bar{b} \gamma^{\mu} \left(f_1^L P_L + f_1^R P_R \right) t - \frac{1}{m_W} \partial_{\nu} W_{\mu}^{-} \bar{b} \sigma^{\mu\nu} \left(f_2^L P_L + f_2^R P_R \right) t \right] + \text{h.c.}$$

Couplings $f_i^L, f_i^R, i = 1, 2$, can be complex in general. In the SM, $f_1^L = 1$ and other couplings are 0.

The EM interaction of spin 1/2 nucleons has a similar form:

$$L_{\gamma NN} = e A_{\mu} \bar{N}(p') \left[\gamma^{\mu} F_1(Q^2) + \frac{i}{2m_N} \sigma^{\mu\nu} q_{\nu} F_2(Q^2) \right] N(p).$$

Form factors $F_1(Q^2)$ and $F_2(Q^2)$, where $Q^2 = -(p - p')^2$, have been adopted from PHOKARA. (Thanks to Szymon and Henryk.)

Anomalous Wtb coupling

The effective Lagrangian of the Wtb interaction containing operators of dimension four and five has the following form:

$$L_{Wtb} = \frac{g}{\sqrt{2}} V_{tb} \left[W_{\mu}^{-} \bar{b} \gamma^{\mu} \left(f_1^L P_L + f_1^R P_R \right) t - \frac{1}{m_W} \partial_{\nu} W_{\mu}^{-} \bar{b} \sigma^{\mu\nu} \left(f_2^L P_L + f_2^R P_R \right) t \right] + \text{h.c.}$$

Couplings $f_i^L, f_i^R, i = 1, 2$, can be complex in general. In the SM, $f_1^L = 1$ and other couplings are 0.

The EM interaction of spin 1/2 nucleons has a similar form:

$$L_{\gamma NN} = e A_{\mu} \bar{N}(p') \left[\gamma^{\mu} F_1(Q^2) + \frac{i}{2m_N} \sigma^{\mu\nu} q_{\nu} F_2(Q^2) \right] N(p).$$

Form factors $F_1(Q^2)$ and $F_2(Q^2)$, where $Q^2 = -(p - p')^2$, have been adopted from PHOKARA. (Thanks to Szymon and Henryk.)

⇒ Simulation of processes involving the EM interaction of nucleons.

Anomalous Wtb coupling

The effective Lagrangian of the Wtb interaction containing operators of dimension four and five has the following form:

$$L_{Wtb} = \frac{g}{\sqrt{2}} V_{tb} \left[W_{\mu}^{-} \bar{b} \gamma^{\mu} \left(f_1^L P_L + f_1^R P_R \right) t \right. \\ \left. - \frac{1}{m_W} \partial_{\nu} W_{\mu}^{-} \bar{b} \sigma^{\mu\nu} \left(f_2^L P_L + f_2^R P_R \right) t \right] + \text{h.c.}$$

Couplings $f_i^L, f_i^R, i = 1, 2$, can be complex in general. In the SM, $f_1^L = 1$ and other couplings are 0.

The EM interaction of spin 1/2 nucleons has a similar form:

$$L_{\gamma NN} = e A_{\mu} \bar{N}(p') \left[\gamma^{\mu} F_1(Q^2) + \frac{i}{2m_N} \sigma^{\mu\nu} q_{\nu} F_2(Q^2) \right] N(p).$$

Form factors $F_1(Q^2)$ and $F_2(Q^2)$, where $Q^2 = -(p - p')^2$, have been adopted from PHOKARA. (Thanks to Szymon and Henryk.)

⇒ Simulation of processes involving the EM interaction of nucleons.

Scalar electrodynamics (sQED)

sQED allows to describe effectively the low energetic EM interaction of charged pions. At low energies, π^\pm can be treated as point like particles represented by a complex scalar field φ .

Scalar electrodynamics (sQED)

sQED allows to describe effectively the low energetic EM interaction of charged pions. At low energies, π^\pm can be treated as point like particles represented by a complex scalar field φ . The $U(1)$ gauge invariant Lagrangian of sQED implemented in carlomat has the form:

$$\begin{aligned}\mathcal{L}_\pi^{\text{sQED}} = & \partial_\mu\varphi(\partial^\mu\varphi)^* - m_\pi^2\varphi\varphi^* - ie(\varphi^*\partial_\mu\varphi - \varphi\partial_\mu\varphi^*)A^\mu \\ & + e^2g_{\mu\nu}\varphi\varphi^*A^\mu A^\nu.\end{aligned}$$

Scalar electrodynamics (sQED)

sQED allows to describe effectively the low energetic EM interaction of charged pions. At low energies, π^\pm can be treated as point like particles represented by a complex scalar field φ . The $U(1)$ gauge invariant Lagrangian of sQED implemented in carlomat has the form:

$$\mathcal{L}_\pi^{\text{sQED}} = \partial_\mu \varphi (\partial^\mu \varphi)^* - m_\pi^2 \varphi \varphi^* - ie (\varphi^* \partial_\mu \varphi - \varphi \partial_\mu \varphi^*) A^\mu + e^2 g_{\mu\nu} \varphi \varphi^* A^\mu A^\nu.$$

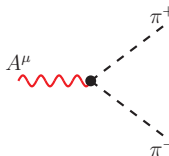
Vertices of sQED:

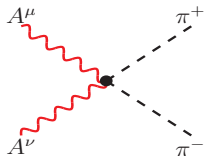
Scalar electrodynamics (sQED)

sQED allows to describe effectively the low energetic EM interaction of charged pions. At low energies, π^\pm can be treated as point like particles represented by a complex scalar field ϕ . The $U(1)$ gauge invariant Lagrangian of sQED implemented in carlomat has the form:

$$\mathcal{L}_\pi^{\text{sQED}} = \partial_\mu \phi (\partial^\mu \phi)^* - m_\pi^2 \phi \phi^* - ie (\phi^* \partial_\mu \phi - \phi \partial_\mu \phi^*) A^\mu + e^2 g_{\mu\nu} \phi \phi^* A^\mu A^\nu.$$

Vertices of sQED:


$$\equiv ie(p_+ - p_-)^\mu$$

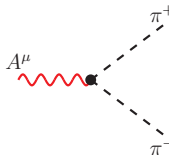

$$\equiv 2ie^2 g^{\mu\nu}$$

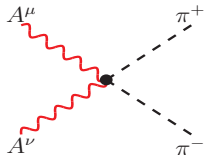
Scalar electrodynamics (sQED)

sQED allows to describe effectively the low energetic EM interaction of charged pions. At low energies, π^\pm can be treated as point like particles represented by a complex scalar field ϕ . The $U(1)$ gauge invariant Lagrangian of sQED implemented in carlomat has the form:

$$\mathcal{L}_\pi^{\text{sQED}} = \partial_\mu \phi (\partial^\mu \phi)^* - m_\pi^2 \phi \phi^* - ie (\phi^* \partial_\mu \phi - \phi \partial_\mu \phi^*) A^\mu + e^2 g_{\mu\nu} \phi \phi^* A^\mu A^\nu.$$

Vertices of sQED:


$$\equiv ie(p_+ - p_-)^\mu$$


$$\equiv 2ie^2 g^{\mu\nu}$$

Vertices of sQED

The bound state nature of the charged pion can be taken into account by the substitutions:

$$e \rightarrow eF_\pi(q^2), \quad e^2 \rightarrow e^2 |F_\pi(q^2)|^2,$$

where $F_\pi(q^2)$ is the charged pion form factor (not implemented).
Implementation of new triple vertices, as e.g.

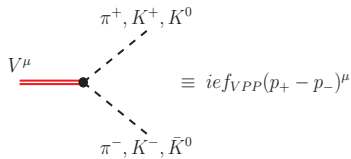
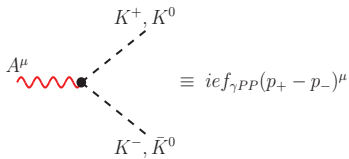
Vertices of sQED

The bound state nature of the charged pion can be taken into account by the substitutions:

$$e \rightarrow eF_\pi(q^2), \quad e^2 \rightarrow e^2 |F_\pi(q^2)|^2,$$

where $F_\pi(q^2)$ is the charged pion form factor (not implemented).

Implementation of new triple vertices, as e.g.



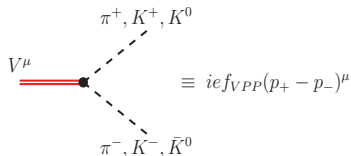
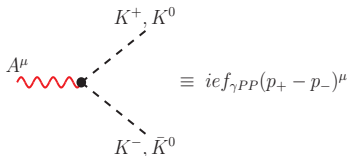
Vertices of sQED

The bound state nature of the charged pion can be taken into account by the substitutions:

$$e \rightarrow eF_\pi(q^2), \quad e^2 \rightarrow e^2 |F_\pi(q^2)|^2,$$

where $F_\pi(q^2)$ is the charged pion form factor (not implemented).

Implementation of new triple vertices, as e.g.



with $V = \rho, \omega, \phi$, or

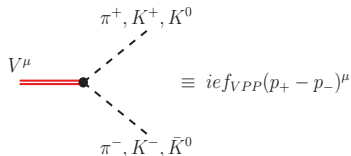
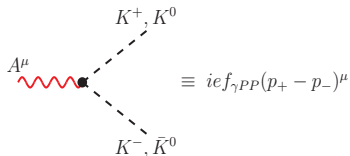
Vertices of sQED

The bound state nature of the charged pion can be taken into account by the substitutions:

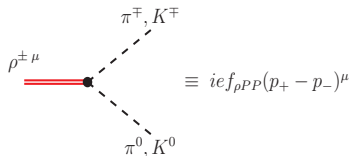
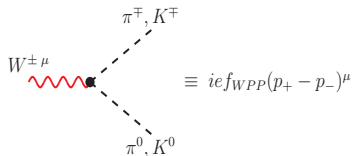
$$e \rightarrow eF_\pi(q^2), \quad e^2 \rightarrow e^2 |F_\pi(q^2)|^2,$$

where $F_\pi(q^2)$ is the charged pion form factor (not implemented).

Implementation of new triple vertices, as e.g.



with $V = \rho, \omega, \phi$, or



is straightforward.

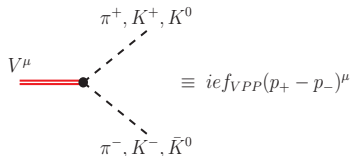
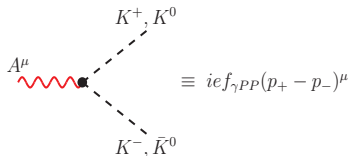
Vertices of sQED

The bound state nature of the charged pion can be taken into account by the substitutions:

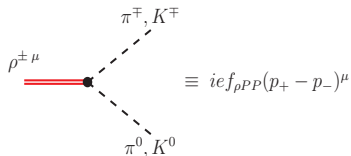
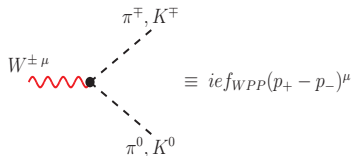
$$e \rightarrow eF_\pi(q^2), \quad e^2 \rightarrow e^2 |F_\pi(q^2)|^2,$$

where $F_\pi(q^2)$ is the charged pion form factor (not implemented).

Implementation of new triple vertices, as e.g.



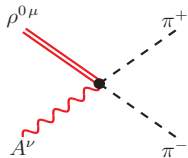
with $V = \rho, \omega, \phi$, or



is straightforward.

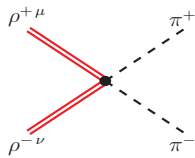
Vertices of sQED and particle mixing

Similarly, quartic vertices such as:



A Feynman diagram showing a quartic vertex. On the left, a red wavy line labeled A^ν and a red double line labeled $\rho^{0\mu}$ meet at a central black dot. On the right, two dashed lines labeled π^+ and π^- emerge from the dot.

$$\equiv 2ieg_{\rho\pi\pi}g^{\mu\nu}$$



A Feynman diagram showing a quartic vertex. On the left, a red double line labeled $\rho^{+\mu}$ and a red double line labeled $\rho^{-\nu}$ meet at a central black dot. On the right, two dashed lines labeled π^+ and π^- emerge from the dot.

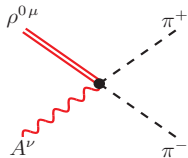
$$\equiv 2ig_{\rho\pi\pi}^2g^{\mu\nu}$$

can also be implemented in a straightforward manner.

Implementation of the particle mixing such as, e.g.

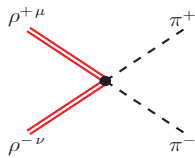
Vertices of sQED and particle mixing

Similarly, quartic vertices such as:



A Feynman diagram showing a central black vertex. A red wavy line labeled A^ν enters from the bottom-left. A red double line labeled $\rho^{0\mu}$ enters from the top-left. A dashed black line labeled π^+ exits to the top-right. A dashed black line labeled π^- exits to the bottom-right.

$$\equiv 2ie g_{\rho\pi\pi} g^{\mu\nu}$$




A Feynman diagram showing a central black vertex. A red double line labeled $\rho^{+\mu}$ enters from the top-left. A red double line labeled $\rho^{-\nu}$ enters from the bottom-left. A dashed black line labeled π^+ exits to the top-right. A dashed black line labeled π^- exits to the bottom-right.

$$\equiv 2ig_{\rho\pi\pi}^2 g^{\mu\nu}$$


can also be implemented in a straightforward manner.

Implementation of the particle mixing such as, e.g.



A Feynman diagram showing a central black vertex. A red wavy line labeled A^μ enters from the left. A red double line labeled $\rho^{0\nu}$ enters from the right.

$$\equiv -ef_{\gamma V} g^{\mu\nu}$$



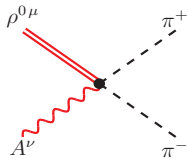
A Feynman diagram showing a central black vertex. A red wavy line labeled $W^{\pm\mu}$ enters from the left. A red double line labeled $\rho^{\mp\nu}$ enters from the right.

$$\equiv -ef_{W\pm\rho^\mp} g^{\mu\nu}$$

is more challenging.

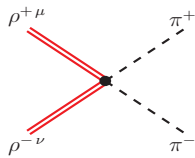
Vertices of sQED and particle mixing

Similarly, quartic vertices such as:



A Feynman diagram showing a quartic vertex. On the left, a red wavy line labeled A^ν and a red double line labeled $\rho^{0\mu}$ meet at a black dot. On the right, a dashed line labeled π^+ and a dashed line labeled π^- meet at the same black dot.

$$\equiv 2ieg_{\rho\pi\pi}g^{\mu\nu}$$




A Feynman diagram showing a quartic vertex. On the left, a red double line labeled $\rho^{+\mu}$ and a red double line labeled $\rho^{-\nu}$ meet at a black dot. On the right, a dashed line labeled π^+ and a dashed line labeled π^- meet at the same black dot.

$$\equiv 2ig_{\rho\pi\pi}^2g^{\mu\nu}$$


can also be implemented in a straightforward manner.

Implementation of the particle mixing such as, e.g.



A Feynman diagram showing a vertex. On the left, a red wavy line labeled A^μ meets a red double line labeled $\rho^{0\nu}$ at a black dot.

$$\equiv -ef_{\gamma V}g^{\mu\nu}$$



A Feynman diagram showing a vertex. On the left, a red wavy line labeled $W^{\pm\mu}$ meets a red double line labeled $\rho^{\mp\nu}$ at a black dot.

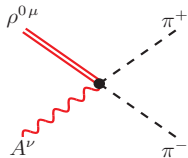
$$\equiv -ef_{W^\pm\rho^\mp}g^{\mu\nu}$$

is more challenging.

Substantial changes in the code generating part of the program are required.

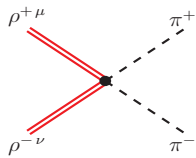
Vertices of sQED and particle mixing

Similarly, quartic vertices such as:



A Feynman diagram showing a quartic vertex. On the left, a red wavy line labeled A^ν and a red double line labeled $\rho^{0\mu}$ meet at a black dot. On the right, a dashed line labeled π^+ and a dashed line labeled π^- meet at the same black dot.

$$\equiv 2ieg_{\rho\pi\pi}g^{\mu\nu}$$




A Feynman diagram showing a quartic vertex. On the left, a red double line labeled $\rho^{+\mu}$ and a red double line labeled $\rho^{-\nu}$ meet at a black dot. On the right, a dashed line labeled π^+ and a dashed line labeled π^- meet at the same black dot.

$$\equiv 2ig_{\rho\pi\pi}^2g^{\mu\nu}$$


can also be implemented in a straightforward manner.

Implementation of the particle mixing such as, e.g.



A Feynman diagram showing a vertex. On the left, a red wavy line labeled A^μ meets a red double line labeled $\rho^{0\nu}$ at a black dot.

$$\equiv -ef_{\gamma V}g^{\mu\nu}$$



A Feynman diagram showing a vertex. On the left, a red wavy line labeled $W^{\pm\mu}$ meets a red double line labeled $\rho^{\mp\nu}$ at a black dot.

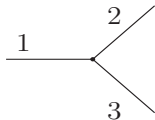
$$\equiv -ef_{W^\pm\rho^\mp}g^{\mu\nu}$$

is more challenging.

Substantial changes in the code generating part of the program are required.

Topology generation in carlomat

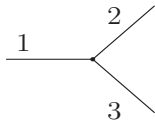
Topologies are generated for models with **triple** and **quartic** couplings, starting with **1 topology** of a **3 particle** process.



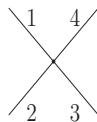
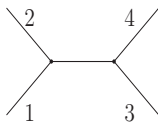
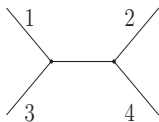
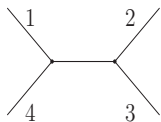
Line 4 is attached to **each line** and to **the vertex** \Rightarrow **4 topologies** of a **4 particle** process.

Topology generation in carlomat

Topologies are generated for models with **triple** and **quartic** couplings, starting with **1 topology** of a **3 particle** process.

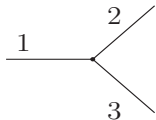


Line 4 is attached to **each line** and to **the vertex** \Rightarrow **4 topologies** of a **4 particle** process.

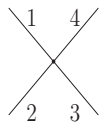
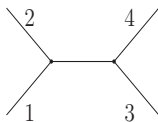
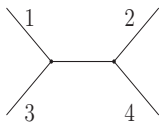
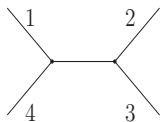


Topology generation in carlomat

Topologies are generated for models with **triple** and **quartic** couplings, starting with **1 topology** of a **3 particle** process.



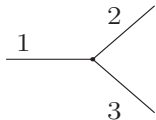
Line 4 is attached to **each line** and to **the vertex** \Rightarrow **4 topologies** of a **4 particle** process.



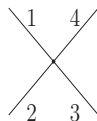
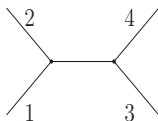
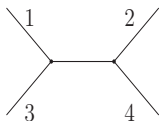
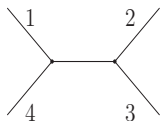
Line 5 is attached to **each line**, including the internal ones, and to each **triple vertex** \Rightarrow **25 topologies** of a **5 particle** process.

Topology generation in carlomat

Topologies are generated for models with **triple** and **quartic** couplings, starting with **1 topology** of a **3 particle** process.



Line 4 is attached to **each line** and to **the vertex** \Rightarrow **4 topologies** of a **4 particle** process.



Line 5 is attached to **each line**, including the internal ones, and to each **triple vertex** \Rightarrow **25 topologies** of a **5 particle** process.

of topologies grows dramatically with # of external particles.

# of particles	# of topologies
6	220
7	2 485
8	34 300
9	559 405
10	10 525 900
11	224 449 225

n external particles \Rightarrow topologies for $n - 1$ particles needed

of topologies grows dramatically with # of external particles.

# of particles	# of topologies
6	220
7	2 485
8	34 300
9	559 405
10	10 525 900
11	224 449 225

n external particles \Rightarrow topologies for $n - 1$ particles needed
 \Rightarrow Feynman rules checked while adding the n -th particle.

of topologies grows dramatically with # of external particles.

# of particles	# of topologies
6	220
7	2 485
8	34 300
9	559 405
10	10 525 900
11	224 449 225

n external particles \Rightarrow topologies for $n - 1$ particles needed
 \Rightarrow Feynman rules checked while adding the n -th particle.

The particle mixing is added just at this stage.

of topologies grows dramatically with # of external particles.

# of particles	# of topologies
6	220
7	2 485
8	34 300
9	559 405
10	10 525 900
11	224 449 225

n external particles \Rightarrow topologies for $n - 1$ particles needed
 \Rightarrow Feynman rules checked while adding the n -th particle.

The particle mixing is added just at this stage.

Vertices of the Resonance Chiral Perturbation Theory (RChPT):

$$\pi^0 \text{---} \bullet \begin{cases} A^\mu(k_1) \\ A^\nu(k_2) \end{cases} \equiv e^2 g_{\pi\gamma\gamma} \varepsilon^{\mu\nu\alpha\beta} k_{1\alpha} k_{2\beta}$$

$$\pi^0 \text{---} \bullet \begin{cases} A^\mu(k_1) \\ \rho^{0\nu}(k_2) \end{cases} \equiv i e g_{\pi^0\gamma\rho^0} \varepsilon^{\mu\nu\alpha\beta} k_{1\alpha} k_{2\beta}$$

$$\begin{matrix} \pi^0 & & \pi^+ \\ & \bullet & \\ A^\mu & & \pi^- \end{matrix} \equiv -e g_{\gamma\pi\pi\pi} \varepsilon^{\mu\nu\alpha\beta} k_{0\nu} k_{+\alpha} k_{-\beta}$$

$$\begin{matrix} \pi^0 & & \pi^+ \\ & \bullet & \\ \rho^{0\mu} & & \pi^- \end{matrix} \equiv -e g_{\omega\pi\pi\pi} \varepsilon^{\mu\nu\alpha\beta} k_{0\nu} k_{+\alpha} k_{-\beta}$$

Their implementation in the program required just a few new subroutines for computation of the corresponding helicity amplitudes.

At the moment, all the form factors are set to 1 or e .

They should be implemented soon in collaboration with Fred Jegerlehner, who provided me with the Feynman rules of the RChPT.

At the moment, all the form factors are set to 1 or e .

They should be implemented soon in collaboration with Fred Jegerlehner, who provided me with the Feynman rules of the RChPT.

Thank you for your attention

At the moment, all the form factors are set to 1 or e .

They should be implemented soon in collaboration with Fred Jegerlehner, who provided me with the Feynman rules of the RChPT.

Thank you for your attention